Subject-specific modulation of local field potential spectral power during brain–machine interface control in primates

2014 J. Neural Eng. 11 026002

(http://iopscience.iop.org/1741-2552/11/2/026002)

IOP Publishing Journal of Neural Engineering
J. Neural Eng. **11** (2014) 026002 (12pp) doi:10.1088/1741-2560/11/2/026002

Subject-specific modulation of local field potential spectral power during brain–machine interface control in primates

Kelvin So[1,5], **Siddharth Dangi**[1,5], **Amy L Orsborn**[2], **Michael C Gastpar**[1,3] **and Jose M Carmena**[1,2,4]

[1] Department of Electrical Engineering and Computer Sciences, University of California, Berkeley, CA, USA
[2] UCB/UCSF Joint Graduate Group in Bioengineering, University of California, Berkeley, CA, USA
[3] School of Computer and Communication Sciences, École Polytechnique Fédérale (EPFL), Lausanne, Switzerland
[4] Helen Wills Neuroscience Institute, University of California, Berkeley, CA, USA

E-mail: carmena@eecs.berkeley.edu

Received 16 September 2013, revised 8 December 2013
Accepted for publication 20 December 2013
Published 6 February 2014

Abstract

Objective. Intracortical brain–machine interfaces (BMIs) have predominantly utilized spike activity as the control signal. However, an increasing number of studies have shown the utility of local field potentials (LFPs) for decoding motor related signals. Currently, it is unclear how well different LFP frequencies can serve as features for continuous, closed-loop BMI control. *Approach.* We demonstrate 2D continuous LFP-based BMI control using closed-loop decoder adaptation, which adapts decoder parameters to subject-specific LFP feature modulations during BMI control. We trained two macaque monkeys to control a 2D cursor in a center-out task by modulating LFP power in the 0–150 Hz range. *Main results.* While both monkeys attained control, they used different strategies involving different frequency bands. One monkey primarily utilized the low-frequency spectrum (0–80 Hz), which was highly correlated between channels, and obtained proficient performance even with a single channel. In contrast, the other monkey relied more on higher frequencies (80–150 Hz), which were less correlated between channels, and had greater difficulty with control as the number of channels decreased. We then restricted the monkeys to use only various sub-ranges (0–40, 40–80, and 80–150 Hz) of the 0–150 Hz band. Interestingly, although both monkeys performed better with some sub-ranges than others, they were able to achieve BMI control with all sub-ranges after decoder adaptation, demonstrating broad flexibility in the frequencies that could potentially be used for LFP-based BMI control. *Significance.* Overall, our results demonstrate proficient, continuous BMI control using LFPs and provide insight into the subject-specific spectral patterns of LFP activity modulated during control.

Keywords: brain–machine interfaces (BMI), local field potential (LFP), primate

S Online supplementary data available from stacks.iop.org/JNE/11/026002/mmedia

(Some figures may appear in colour only in the online journal)

[5] Kelvin So and Siddharth Dangi contributed equally to this work.

1. Introduction

Brain–machine interfaces (BMIs) hold potential to restore motor function in patients with severe neurological conditions by enabling control of external devices via modulation of neural activity [1]. Intracortical BMI studies have traditionally used single- and multi-unit activity as control signals, due to the fact that the discharge of motor cortical neurons correlates with different movement parameters, and that these cells can be volitionally modulated irrespective of physical movement using biofeedback [2]. On the other hand, certain features of local field potentials (LFPs), which are the extracellular potentials resulting from the synaptic activity in a neuronal population, have also been shown to exhibit similar tuning properties [3]. For instance, initiation of arm movement has been shown to reliably modulate power in the LFP beta band (∼15–30 Hz) [4]. In addition, other studies have shown that muscle activity, eye movements, and reaching and grasping kinematics can all be decoded from LFP activity to varying degrees of accuracy [5–7]. This makes LFPs an attractive alternative to single- and multi-unit activity in BMIs because they are more robust to signal degradation over time [8] and contain more information than other less invasive field potentials such as electroencephalography (EEG) and electrocorticography (ECoG) signals.

Despite the promising properties of LFPs for BMI control, only a few studies to date have used them explicitly as an input signal in BMIs [9–11], with one study demonstrating 2D continuous BMI control [11]. In that study, Flint *et al* trained decoders offline biomimetically (using neural activity recorded during overt arm movements) and held them fixed thereafter. While proficient BMI control was achieved in this way, the biomimetic approach may constrain the subject to modulate neural activity during a closed-loop BMI task in a way similar to activity evoked during natural arm movements. For instance, a low frequency feature known as the local motor potential (LMP) has been found to be informative in decoding kinematic parameters of arm-related movements [12], and Flint *et al* indeed reported that the LMP and the 0–4 Hz band were the most informative features for LFP-based BMI control [13]. However, little is known about the degree of flexibility of the brain to modulate LFP oscillations of higher frequencies, or whether a broader range of frequencies can be used for BMI control with LFPs.

Here, we apply closed-loop decoder adaptation (CLDA) [14] during LFP-based BMI control to adapt the decoder to subject-specific modulations of different LFP frequency bands. Using CLDA in combination with an assistive control paradigm, we trained two non-human primates to perform a center-out task using LFP activity in the 0–150 Hz range. We then analyzed the relative importance of the different frequency bands toward each monkey's cursor control. While both monkeys obtained proficient control of the cursor under identical task settings, the frequency bands most important to control were characteristically different between both monkeys. Next, we constrained the BMI control input to various frequency sub-ranges (0–40 , 40–80 , and 80–150 Hz) and found that our offline analyses accurately predicted the bands with which the monkeys achieved the best online performance. Interestingly, while each monkey performed better using certain frequency ranges, both monkeys were able to achieve BMI control well above chance level with all sub-ranges after decoder adaptation, suggesting that broad ranges of LFP frequencies can potentially be used for closed-loop BMI control. Finally, we found that the particular frequency bands most important for each subject's control influenced the number of channels they needed, due to differences in the correlations across channels at different frequencies. Overall, our results demonstrate proficient, continuous BMI control using LFPs and shed light on the range of frequencies that can potentially be used, with implications for channel and feature selection.

2. Materials and methods

2.1. Electrophysiology and behavioral task

Two adult male rhesus macaques (*macaca mulatta*) were chronically implanted in the brain with bilateral microwire arrays of 128 Teflon-coated tungsten electrodes (35 μm diameter, 500 μm wire spacing, 8×16 array configuration; Innovative Neurophysiology, Durham, NC), targeting the arm areas of primary motor cortex (M1) and dorsal premotor cortex (PMd). All procedures were conducted in compliance with the NIH Guide for Care and Use of Laboratory Animals and were approved by the University of California–Berkeley Institutional Animal Care and Use Committee.

LFP signals were sampled at 1 kHz using a 128-channel MAP recording system (Plexon Inc., Dallas, TX) and streamed to a dedicated computer running MATLAB (The Mathworks, Natick, MA) to implement feature extraction and closed-loop BMI control. Channels were referenced to ground and signal quality was visually inspected each day (channels with clear artifacts were removed). For each channel, we estimated the spectral power in 15 consecutive 10 Hz bands from 0–150 Hz using the multi-taper method [15]. Spectral estimation was performed every 100 ms using a sliding window containing the most recent 200 ms of raw LFP activity. The estimates of log spectral power in different frequency bands, across multiple LFP channels, were used as neural features for closed-loop BMI control (figure 1(A)).

The monkeys were head-restrained in a primate chair as they performed a self-paced 2D center-out task. Monkeys were previously trained to perform this task by performing reaches using their right arm. During BMI control, the monkeys did not perform these arm reaches, as their arms were confined within the primate chair. Trials were initiated by moving the cursor under neural control to the center target and holding for 300 ms, after which the monkeys had to reach to one of eight peripheral targets uniformly spaced about a 13 cm diameter circle and hold for 400 ms to receive a liquid reward (target radii = 1.7 cm). The monkeys were then required to move the cursor back to the center target to initiate the next trial. If the monkeys failed to hold or reach the target within 10 s, the trial was restarted without reward (figure 1(B)).

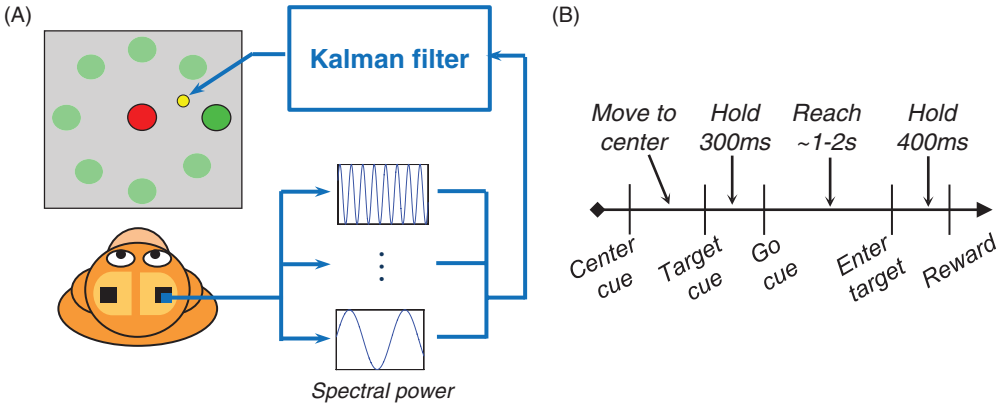

Figure 1. *Experimental setup.* (A) Illustration of the BMI task set-up. (B) Trial timeline for the BMI center-out task.

2.2. Brain–machine interface

A Kalman filter (KF) decoding algorithm ('decoder') was used to implement closed-loop BMI control. The KF assumes the following models for how the kinematic state of the cursor (x_t) evolves over time and how the observed vector of extracted LFP features (y_t) relates to the state:

$$x_t = Ax_{t-1} + w_t \quad (1)$$

$$y_t = Cx_t + q_t \quad (2)$$

where $w_t \sim \mathcal{N}(0, W)$ and $q_t \sim \mathcal{N}(0, Q)$ are additive Gaussian noise terms. At each iteration, the KF estimates x_t using y_t and its previous estimate of x_{t-1} (see [16] for the actual filter equations that perform the state estimation at each iteration). While there is no explicit delay between the kinematic state and neural activity in the KF model, each measurement y_t contains information from neural activity up to 200 ms in the past.

We used a position-velocity KF, in which the KF state vector x_t is defined to include the position (p) and velocity (v) of the cursor at time t, along both the horizontal and vertical directions of the screen:

$$x_t = [p_{\text{horizontal},t} \quad p_{\text{vertical},t} \quad v_{\text{horizontal},t} \quad v_{\text{vertical},t} \quad 1]^T.$$

The constant term 1 and a corresponding extra column of C are added to account for neural observations y_t with non-zero means. The structures of A and W were constrained as in [17] such that integrating the velocity from one KF iteration perfectly explains position at the next iteration. C and Q were initially constructed by shuffling the rows and columns of a previous set of C and Q matrices that were trained with native arm reaches from the subject. These initial parameters were then updated during closed-loop BMI operation using the SmoothBatch CLDA algorithm (see section 2.3). We typically adapted these parameters only during initial closed-loop control, and did not perform additional CLDA on the same decoder throughout the rest of the experiment.

In addition to producing estimates of the state vector x_t, the KF also generates an error covariance matrix P_t at each time-step that represents the filter's confidence in its own state estimates. Specifically, the diagonal terms of P_t represent the KF's error variances for its estimates of the state vector variables (i.e., larger values reflect lower confidence). Note that during standard operation of the filter, P_t quickly converges to a steady-state matrix P that depends only the model parameters (A, W, C, Q).

During the first training session of each experiment, we utilized an assistive control paradigm [18] simultaneously with CLDA. After decoder initialization, the cursor was temporarily assisted toward the target. Specifically, the cursor trajectory was determined by:

$$\overrightarrow{v_{\text{cursor}}} = \alpha \cdot \overrightarrow{v_{\text{assist}}} + (1 - \alpha) \cdot \overrightarrow{v_{\text{user}}}$$

where $\overrightarrow{v_{\text{user}}}$ is the decoded output from the KF, $\overrightarrow{v_{\text{assist}}}$ is a vector that points directly toward the current target, and $\overrightarrow{v_{\text{cursor}}}$ is a weighted average of the two that determines the final cursor output shown to the subject. The weighted average was set by the assist level $\alpha \in [0, 1]$, which was manually adjusted in real-time depending on the subject's performance (at $\alpha = 0$, the cursor was fully controlled by the subject). The assist speed was set to 0.8 cm s^{-1} to match the natural speed of the cursor when the subject performed the center-out task under manual control. All analyses were performed on data with the cursor under full volitional control (0% assist).

2.3. Closed-loop decoder adaptation

CLDA is an emerging paradigm for improving or maintaining the online performance of BMIs. By adapting the decoder's parameters during closed-loop BMI operation (i.e., while the subject is using the BMI), CLDA algorithms aim to match the decoder's output to the subject's particular pattern of neural activity [17, 19–27]. In our experiments, we used the SmoothBatch CLDA algorithm to adapt the KF decoder's parameters during initial closed-loop control. The SmoothBatch CLDA algorithm has been previously used in spike-based BMI experiments, where it was demonstrated to rapidly improve BMI performance independent of the decoder's initialization method [26]. Furthermore, SmoothBatch has also been shown to possess a variety of favorable algorithmic convergence properties [14].

To illustrate how the SmoothBatch CLDA algorithm operates, let $C^{(i-1)}$ and $Q^{(i-1)}$ denote the current observation model parameters of the KF decoder. SmoothBatch first collects a batch of neural activity and cursor kinematics as the subject operates the BMI cursor in closed-loop control

using a decoder with these parameters. Next, the algorithm generates an estimate of the user's intended cursor movements. For example, in our experiments, we used Gilja *et al*'s method for inferring intended cursor kinematics ('innovation 1' of the ReFIT-KF algorithm), which assumes that the subject always intends to move to directly toward the current target [17]. Other methods for estimating intended movements could also be used in conjunction with SmoothBatch, such as Shpigelman *et al*'s supervised method [21] or Li *et al*'s unsupervised method [24]. Using the estimate of intended cursor kinematics and the recorded neural activity, SmoothBatch then constructs batch maximum likelihood estimates, $\hat{C}$ and $\hat{Q}$, of the C and Q matrices using the following equations:

$$\hat{C} = YX^T(XX^T)^{-1} \tag{3}$$

$$\hat{Q} = \frac{1}{N}(Y - \hat{C}X)(Y - \hat{C}X)^T \tag{4}$$

where the Y and X matrices are formed by tiling N columns of recorded neural activity and intended kinematics, respectively. The size of the data batch is parametrized by the batch period $T_b \triangleq N \cdot dt$ (where dt is the time between decoder iterations). Finally, the algorithm updates the observation model parameters using a weighted average:

$$C^{(i)} = (1-\rho)\hat{C}^{(i)} + \rho C^{(i-1)} \tag{5}$$

$$Q^{(i)} = (1-\rho)\hat{Q}^{(i)} + \rho Q^{(i-1)} \tag{6}$$

where i indexes discrete batch periods and the weighting parameter $\rho \in [0, 1]$ controls the influence of $\hat{C}$ and $\hat{Q}$ on the new parameter settings. Note that SmoothBatch does not update the KF transition model parameters A and W. We typically reparametrize ρ in terms of a half-life h (i.e., the time it takes for a previous maximum likelihood estimate's weight in the decoder to be reduced by a factor of 2):

$$\rho^{h/T_b} = \tfrac{1}{2}$$

where T_b is the size of the batch ('batch period') measured in units of time. In our experiments, batch periods and half-lives were typically chosen in the ranges $T_b \in [1, 6]$ min and $h \in [0.5, 15]$ min.

2.4. Performance evaluation

We quantified performance by measuring the target acquisition rate in trials/min and the percentage of initiated trials (those in which the subject was able to hold for 300 ms at the center) that ended in a success, both of which were computed using a five minute sliding window with 30 s steps. For comparison, we estimated the chance rate (measured to be 0.3 trials min^{-1} at a 0% assist level) by simulating 30 min of the task performed using a random walk trajectory (generated with the same transition model parameters as the KFs used for BMI control). We also measured trajectory quality using reach time (RT), normalized path length (NPL), movement error (ME), and movement variability (MV); see [26] for details on each metric.

To perform approximate comparisons of BMI cursor control performance across studies (see section 4), we calculated a summary statistic using the Fitts Law derived index of difficulty, which has been proposed as a standardized assessment method for neural prostheses [28]. The index of difficulty, measured in bits, is calculated based on the distance to target ('Distance') and target diameter ('Window') as:

$$\text{Index of difficulty} = \log_2\left(\frac{\text{Distance} + \text{Window}}{\text{Window}}\right).$$

From this value and the mean RT, we calculate throughput in Fitts bits s^{-1} as:

$$\text{Throughput} = \frac{\text{Index of difficulty}}{\text{Mean reach time}}.$$

We refer the reader to [17] for further details on throughput calculation.

3. Results

During an initial set of experiments, we randomly chose 20 channels from the right M1/PMd implants and extracted the spectral power from fifteen 10 Hz bands, spanning 0–150 Hz, as input features to the decoder. Both animals attained full control of the 2D cursor using CLDA with the assistive control paradigm. Assistive control started at 100% ($\alpha = 1$) and was reduced to zero after day 1 and CLDA was stopped after day 2. Both animals performed the task under full volitional control for two additional days. The target acquisition rate without assist improved from day 2 to 4 for both monkeys (Pearson's correlation coefficient, Monkey S: $R = 0.34$, $p < 0.001$; Monkey J: $R = 0.30$, $p < 0.001$). The average target acquisition rates on the fourth day for Monkey S and Monkey J were 10.6 ± 2.4 trials min^{-1} and 5.8 ± 2.9 trials min^{-1}, respectively. The average success percentage was $78\% \pm 6\%$ for Monkey S and $72\% \pm 8\%$ for Monkey J. Figure 2(A) shows typical reach trajectories, rate of target acquisition, and chance level for both monkeys on the fourth day of the series.

Trial-averaged spectrograms for each of the eight target directions, along with tuning curves for each frequency band, are shown in figures 2(B)–(C) for the two monkeys. The modulation depth, defined as the difference between the highest and lowest points of the tuning curve, is shown for each frequency in figure 2(D). Monkey S showed highest modulation in the 0–20 Hz frequency range, with another peak in the 50–80 Hz range, but decreasing modulation at higher frequencies. In contrast, Monkey J showed highest modulation depth in both 0–20 Hz and 80–150 Hz range. In addition, the LFP modulations during BMI control were also considerably different than those during natural arm control. Figure 3 shows the trial-averaged spectrograms, tuning curves and modulation depth plots in prior training sessions where Monkey S performed the same center-out task using natural arm reaches (no brain control). The characteristic decrease in beta band (15–40 Hz) power during movement was clearly evident during natural arm movement, but did not occur during BMI control.

Although tuning curves are one representation of the relationship between cursor movement and neural activity, they do not fully capture the exact mechanism by which the cursor position is generated from the neural activity at each iteration, since this is specified by the BMI decoder. To provide

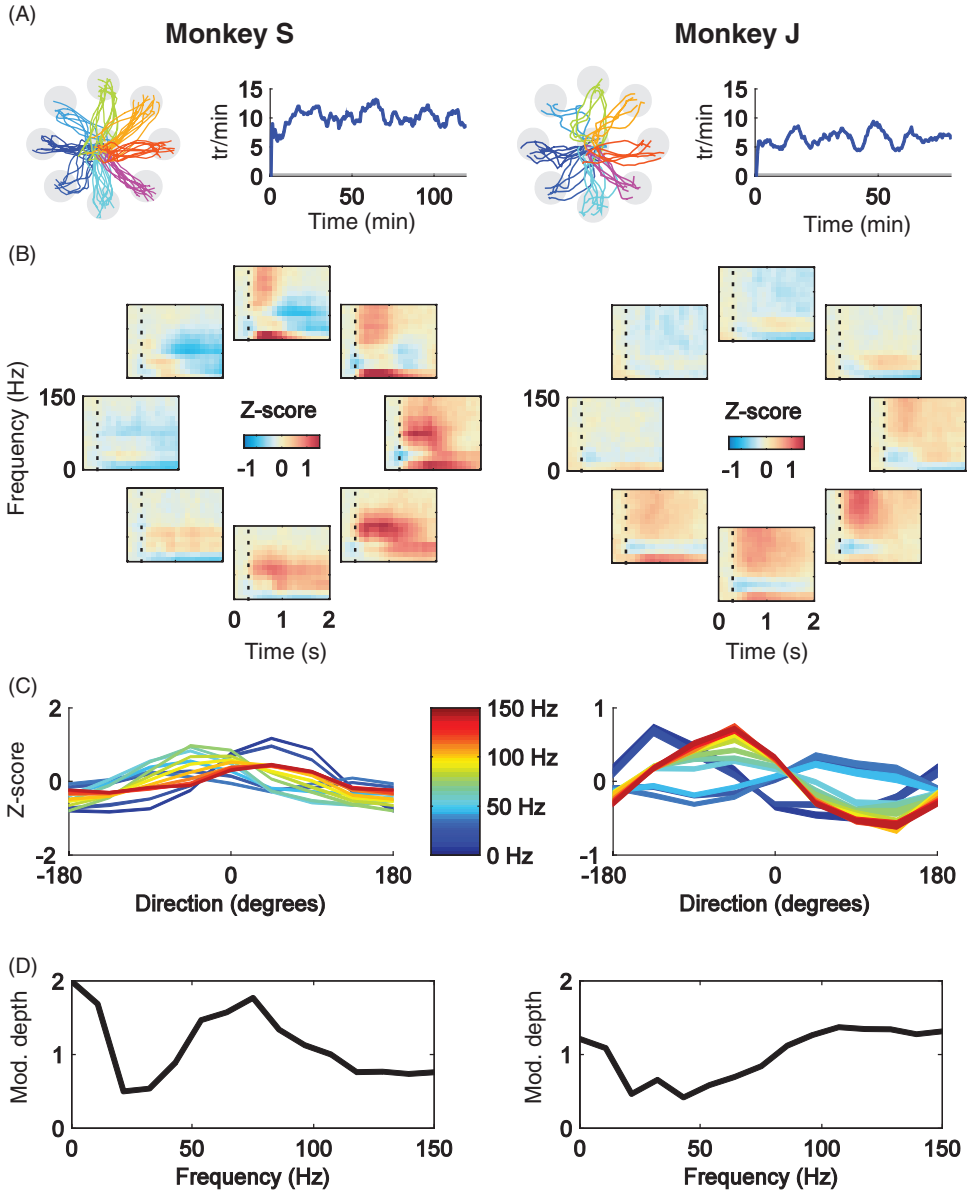

Figure 2. *Neural activity during closed-loop BMI control.* (A) Left: typical reach trajectories to the eight center-out targets on the fourth day of the series for both monkeys. Right: target acquisition rate on fourth day. Gray line indicates chance rate. (B) Trial-averaged spectrograms illustrating the *z*-scored log power on one channel during successful reaches for both subjects. (C) Tuning curves for each of the 15 spectral power features (on one particular channel) used for closed-loop control. Line thickness reflects standard error of the mean. (D) Modulation depth as a function of LFP frequency.

further insight into the LFP activity modulated during control, we examined the KF decoder's observation model parameters (C and Q), which capture the relationship between cursor kinematics and observed neural activity. Since our KF state vector models cursor position and velocity, the rows of C reflect the preferred position and velocity directions of different LFP features. For instance, figure 4(A) illustrates the preferred velocity directions for each 10 Hz frequency band (averaged across channels) as assigned in C. In combination with the covariance structure modeled in Q, these preferred velocities ultimately determine how feature modulations of different features contribute to cursor movement at each iteration. For example, figure 4(B) (top) shows the contributions to the cursor displacement from each LFP frequency band (averaged across channels) during an example trial. Each individual vector represents the net cursor displacement during the reach due to the modulations of a particular frequency band (together, the vectors add to produce the overall cursor displacement). The underlying modulations of neural activity (averaged over the course of the reach) that were generated to create this trajectory are shown in figure 4(B) (bottom). Hence, to generate the trajectory shown, Monkey S increased the 0–20 Hz activity while reducing activity from 30–80 Hz.

In order to identify the LFP frequencies within the 0–150 Hz range that were most important for each monkey's overall BMI control, we calculated a movement contribution profile for each monkey by similarly decomposing the cursor movement across all successful trials. We considered three broad groups of frequencies—0–40 (approximately the delta, theta, mu, and beta bands), 40–80 (low gamma), and

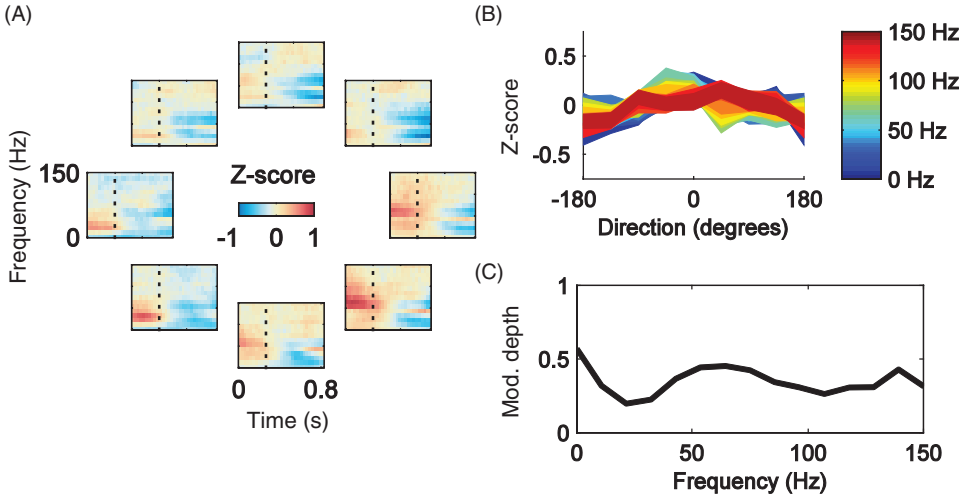

Figure 3. *Neural activity during natural arm movement.* (A) Trial-averaged spectrograms illustrating the z-scored log power on one channel in the contralateral hemisphere during natural right arm reaches in a center-out task for Monkey S. Dotted line indicates the go cue. (B) Tuning curves for each of the 15 spectral power features (on one particular channel). Line thickness reflects standard error of the mean. (C) Modulation depth as a function of LFP frequency.

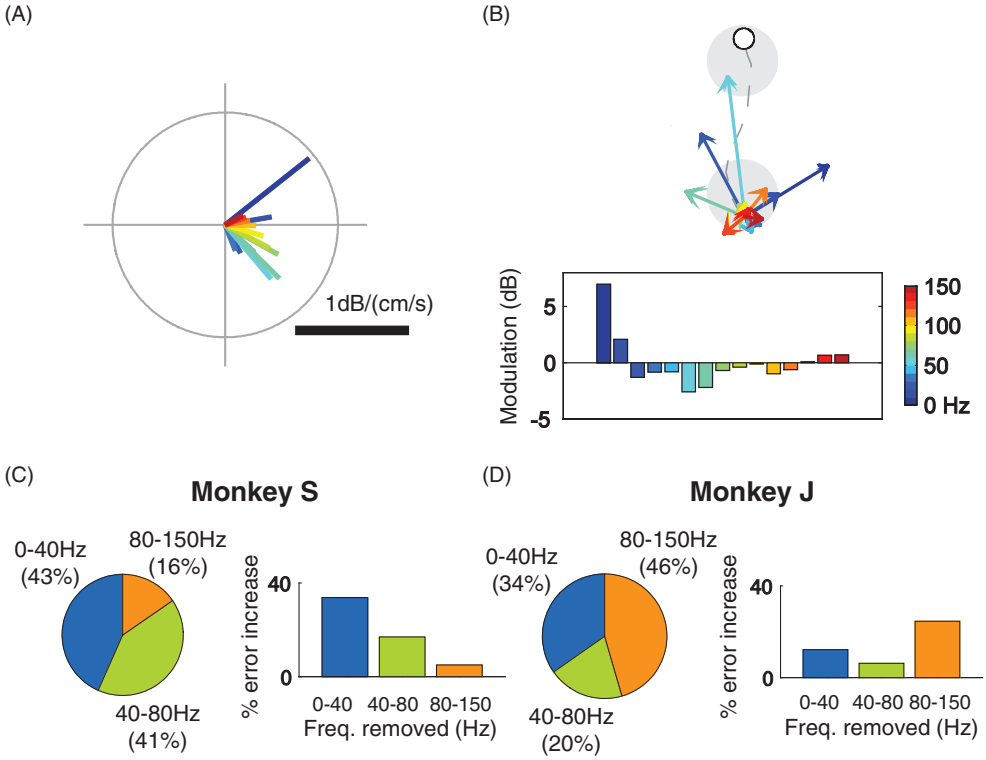

Figure 4. *Importance of different LFP features to closed-loop BMI control.* (A) Preferred velocity directions for each 10 Hz frequency band as assigned in the KF observation model matrix C for Monkey S. (B) Top: cursor trajectory (dashed gray line) during an example reach to the top target. Each colored vector indicates the net cursor displacement during the reach resulting from a particular frequency band. The vectors from all frequency bands add to produce the overall cursor displacement. Bottom: the underlying modulations of neural activity generated during the sample reach. (C–D) Movement contribution profiles (pie charts, left) and sensitivity analyses (bar graphs, right) across three groups of frequencies—0–40, 40–80, and 80–150 Hz, for both monkeys. Movement contribution profiles were calculated by decomposing the subjects' movements on successful trials into contributions from the three groups of frequencies, as in (B, top). Sensitivity analyses reflect increases in the Kalman error variances when certain groups of frequencies are removed from the KF decoder model.

80–150 Hz (high gamma)—and determined the contribution of each frequency group, measured as a percentage of the total displacement. The resulting percentages directly measure which frequencies were responsible for moving the cursor on the screen (figures 4(C)–(D), pie charts). For Monkey S, the 0–40 Hz and 40–80 Hz bands together accounted for an average of 84% of the cursor movement per reach, while the higher frequencies (80–150 Hz) only accounted for 16% of the movement. Interestingly, Monkey J's movement contribution profile was markedly different than that of Monkey S. For

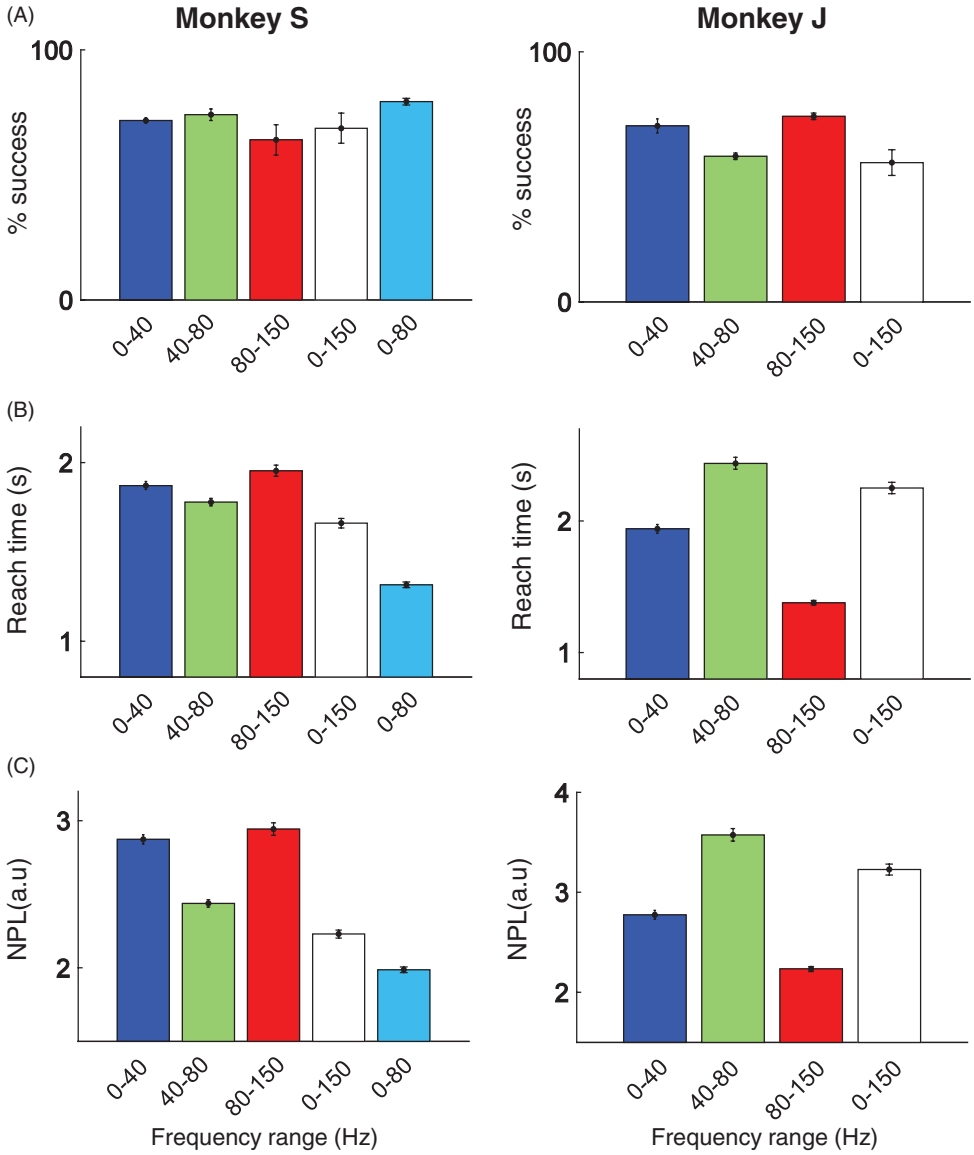

Figure 5. *Closed-loop BMI control with different sub-ranges of LFP frequencies.* Experimental performance, measured using (A) success percentage, (B) reach time (RT, seconds) and (C) normalized path length (NPL, arbitrary units), of both subjects across multiple experimental series in which various sub-ranges of the full 0–150 Hz range were used as neural features for closed-loop control. Bars indicate the mean across the entire series, and error bars indicate standard error of the mean.

Monkey J, the 80–150 Hz and 0–40 Hz bands were most responsible for cursor movement (46% and 34%, respectively).

As another way to measure the importance of different LFP frequencies for closed-loop control, we performed a leave-one-out offline sensitivity analysis by removing frequency groups from the KF decoder model and measuring the resulting increases in the steady-state Kalman error variances. These increases measure the impact on the decoder's confidence in its state estimates if the corresponding features were not used in closed-loop decoding (figures 4(C)–(D), bar graphs). For Monkey S, removing the 0–40 Hz and 40–80 Hz bands resulted in larger increases (34% and 17%) in the Kalman error variances than removing the 80–150 Hz frequencies (5%), suggesting that the 0–80 Hz frequencies were relatively more important. On the contrary, for Monkey J, removing the 80–150 Hz frequencies resulted in the largest increase (25%) in the error variance compared to removing the 0–40 Hz or 40–80 Hz bands (12% and 6% increase, respectively), suggesting that 80–150 Hz was more important than the other two frequency groups for Monkey J.

3.1. Testing different frequency bands

To test the predictions derived from our analyses, we conducted multiple experimental series in which both monkeys were restricted to only use features extracted from various sub-ranges (0–40, 40–80, and 80–150 Hz) of the full 0–150 Hz (from the same 20 channels) for closed-loop BMI control. Each series was composed of 3–4 days, with CLDA and assistive control performed on the first day starting from shuffled decoder parameters as before. On subsequent days, CLDA was used on rare occasions only if performance decreased drastically. Figure 5 depicts both monkeys' performance,

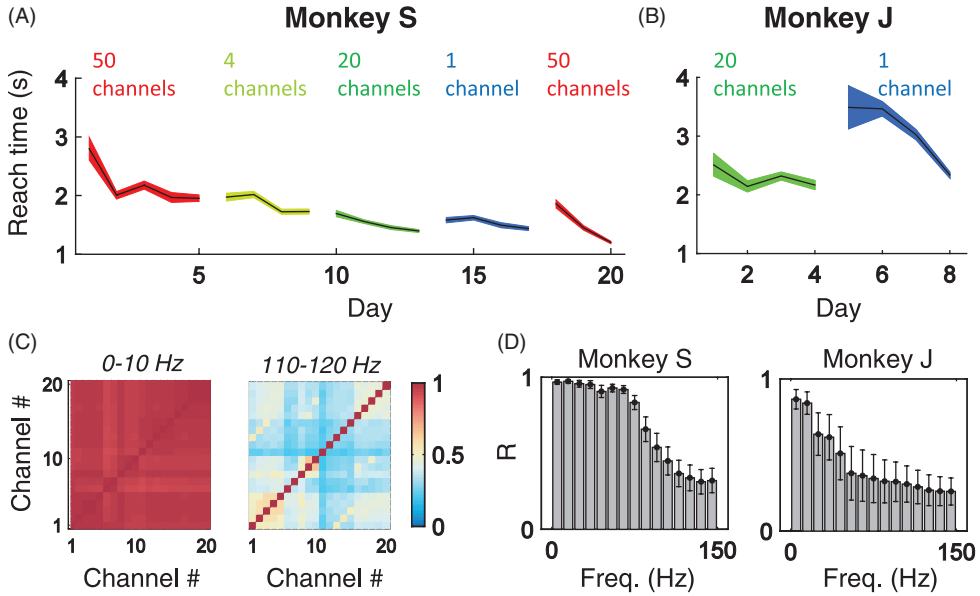

Figure 6. *Closed-loop BMI control with different numbers of LFP channels.* Experimental performance of (A) Monkey S and (B) Monkey J, measured using RT, across multiple experimental series in which varying numbers of LFP channels were used in the decoder for closed-loop control. (C) Correlation matrices for Monkey S depicting the correlations across channels for the 0–10 Hz and 110–120 Hz frequency features (i.e., log power in different frequency bands). (D) Average correlation between features values on different channels for both subjects.

measured using average success percentage, mean RT and NPL, across these multiple frequency series.

Among the three frequency groups, Monkey S performed best in all metrics (success percentage, RT, NPL, MV, and ME) when using 40–80 Hz for closed-loop control. This result is consistent with his movement contribution profile (figure 4(C)), which showed that the 40–80 Hz band accounted for an average of 41% of cursor movement during trials. However, the contribution profile showed that the 0–40 Hz band also accounted for a large percentage of movement (43%), and furthermore, our Kalman sensitivity analysis predicted 0–40 Hz to be the most important band for Monkey S. These analyses suggested that the combination of the two frequency bands (0–40 and 40–80 Hz) might allow Monkey S to achieve a higher level of performance. As such, we conducted an additional frequency series in which Monkey S used 0–80 Hz for control. As expected, with respect to all metrics, Monkey S performed best across all frequency series when using 0–80 Hz. For instance, Monkey S's RTs were significantly lower when using 0–80 Hz than any other band ($p < 0.001$ for comparisons to each of the other four frequency series; Kruskal–Wallis ANOVA). Differences in mean NPL, ME, and MV when using 0–80 Hz versus any other band were also all significant ($p < 0.001$ for ME, MV, and NPL; Kruskal–Wallis ANOVA).

Conversely, among all bands, Monkey J performed best using 80–150 Hz in all metrics ($p < 0.001$ for differences in RT, NPL, ME, and MV; Kruskal–Wallis ANOVA). Indeed, these findings confirm the results of Monkey J's movement contribution profile and Kalman sensitivity analysis, both of which predicted 80–150 Hz to be most important for his cursor control (figure 4(D)). Moreover, just as those analyses had predicted 0–40 Hz to be second most important, Monkey J indeed performed second-best across all frequency series when using 0–40 Hz. Finally, Monkey J performed worst across all metrics when using 40–80 Hz, a result that is also consistent with predictions from the analysis.

Although we found that both monkeys performed better with some frequency sub-ranges than others, it is interesting to note that they were still able to achieve BMI control with all sub-ranges after initial decoder adaptation. Overall, these results suggest that there may be broad flexibility in the frequencies that could potentially be used for closed-loop LFP-based BMI control.

3.2. Testing different numbers of LFP channels

We also investigated the impact of reducing the number of channels on BMI control. Due to the close proximity of adjacent channels on the electrode array, the correlation between the raw LFPs from channels on the same array often exceeds 0.95. Hence, it is possible that multiple channels on the same array may not contribute additional information or degrees of freedom.

We varied the number of channels used for control in Monkey S from 50 channels to 1 channel (all from the right hemisphere, split between M1 and PMd) and tested each configuration for 3–4 days. We found that RTs decreased over time irrespective of the number of channels used (figure 6(A)). We repeated the 50 channel configuration after the last series (1 channel series) and the RTs rapidly approached that of the previous series and kept decreasing. As mentioned above, one reason for the apparent low impact of the number of channels may be due to the high correlation between all LFP channels on a single electrode array. Comparing the power of each frequency band across 20 channels, we found high

correlations between channels at frequencies below 80 Hz, but lower correlations at higher frequencies (figure 6(C)). Since Monkey S relied primarily on modulating frequencies below 80 Hz for control, the redundancy across channels in the input was especially prominent. For Monkey S, our results suggested that the volitional modulation of different frequency bands, from even a single channel, was sufficient for 2D cursor control.

We also tested BMI control in Monkey J with a 20 channel and 1 channel configuration (figure 6(B)). In contrast to Monkey S, Monkey J's initial RTs with 1 channel input were dramatically higher than the 20 channel input series that was used earlier. While the RTs decreased with training, the high initial increase in RTs when switching from 20 channels to a single channel for Monkey J suggested that the removal of channels from the same hemisphere had a greater detrimental effect for Monkey J than for Monkey S. The disparity may result from the difference in frequency bands most important for cursor control between Monkey S and J, and the correlations across channels for those frequency bands. For Monkey J, the 80–150 Hz band accounted for most of the cursor movement, but was also less correlated among channels (figure 6(D)). Hence, there was less redundancy across channels compared to Monkey S, resulting in a greater effect on performance when channels were removed. Overall, we found that the effect of the number of LFP channels used on BMI control can vary depending on the strategy of frequency modulations used by a particular subject.

4. Discussion

By using an adaptive approach (CLDA) to fit decoder parameters, we match the decoder output to the modulations of LFP evoked by the monkeys as they attempted to move the cursor toward the target. This paradigm allows the cursor to be controlled by the specific LFP modulations evoked by the subject during closed-loop BMI control. As a result, while both monkeys were trained on identical task settings, our movement contribution and sensitivity analyses revealed differences between monkeys in the contribution and relative importance of each LFP frequency band. We tested the analysis results empirically by requiring the monkeys to perform the same task using only sub-ranges of the entire 0–150 Hz band. For Monkey S, the 0–40 Hz (delta, theta, mu, and beta bands) and 40–80 Hz (low gamma), contributed significantly to the cursor movement (43% and 41%, respectively) based on the movement contribution profile. Subsequently, Monkey S performed best across all performance metrics when using frequencies 0–80 Hz and worst when these frequencies were removed. In contrast, for Monkey J, the 80–150 Hz (high gamma) range contributed the most out of the three groups to cursor movement in our analysis (46%), and indeed Monkey J performed significantly better across all metrics when using 80–150 Hz for closed-loop control. However, it is interesting to note that both monkeys were able to achieve above chance level performance using *all* of the frequency sub-ranges, even when they didnot include the most important frequency bands for each monkey.

A prior LFP-based BMI study by Flint *et al* also extracted LFP spectral power as neural features, but sub-divided frequencies in a different way: 0–4, 7–20, 70–115, 130–200, and 200–300 Hz [11]. In addition, Flint *et al* utilized the LMP—a very low-pass filtered version of the time-domain LFP signal—as a feature for closed-loop control. In a related initial study [13], Flint *et al* reported that the LMP and the power in the 0–4 Hz band appeared to be among the most informative features for control for both subjects (together, they accounted for 80% and 43% of the features used in their two monkeys). A key difference compared to the current study was that Flint *et al* used a fixed decoder trained from neural activity collected as the monkey performed natural reaches. Since the decoder parameters did not adapt, the subjects may have been constrained to modulate neural activity in ways similar to the activity used to fit the decoder; namely, those generated during natural reaches. Given that the LMP has been shown to be informative in decoding movement trajectories and reach direction [12], it is not surprising that the LMP was found to be the one of the most informative features for control when using a fixed decoder trained from natural reaches. In the current study, the decoder was initialized using a random shuffling method and fit with an adaptive procedure, using neural activity evoked during closed-loop BMI control. Hence, subjects were not constrained to modulate neural activity in a predefined way. The range of informative frequencies in our results indicate that a broader band of LFP frequencies can potentially be effective for closed-loop BMI control. This result is consistent with recent findings that LFP power in the 30–50 Hz range and ECoG power in the 75–105 Hz range can be volitionally modulated during closed-loop BMI in a operant conditioning paradigm [10, 29, 30].

Are there frequencies that are inherently more readily modulated than others in a closed-loop BMI setting? Hwang *et al* [9] reported that LFP power in the 0–10 Hz and 20–40 Hz bands in the parietal reach region could be volitionally modulated to initiate trials. Engelhard *et al* [10] found that the 30–50 Hz band could be robustly modulated when a constraint to use this range is directly imposed. When such constraints are relaxed, our results indicate that the range of frequencies that subjects modulate can vary from subject to subject. One potential reason for the variation may be due to the recording quality of high frequencies from the electrode array. From the time of initial array implantation to the time of the present study, the LFP power in frequencies above 80 Hz decreased by approximately 10 dB for Monkey S (∼3 years post implant) but only 2 dB for Monkey J (∼1.5 years post implant). Hence, the low contribution of the 80–150 Hz band to BMI control for Monkey S may be a result of the low signal-to-noise ratio in that frequency band. Nonetheless, Monkey S was able to obtain control well above the chance level using both these and other frequency bands (e.g., 0–80 Hz), indicating that broad ranges of LFP frequencies can potentially be used for a closed-loop BMI.

While the randomized decoder initialization may have some effect on the subjects' control strategy, we believe this effect to be negligible. The trained decoder that is achieved using the SmoothBatch CLDA algorithm ultimately depends

Table 1. Performance comparison to other BMI cursor reaching studies. Comparison of the BMI performance achieved in this study with a small sampling of recent closed-loop BMI cursor control studies using spikes, LFPs, ECoG, and EEG. Throughput in bits per second is computed by calculating an index of difficulty (measured in bits) based on task settings and dividing by the mean RT (measured in seconds). The index of difficulty of a task is calculated based upon the distance to targets and the target size (see section 2).

Neural signal	Study	Target hold time (ms)	Index of difficulty (bits)	Reach time (s)	Throughput (bits s^{-1})
Spikes	Taylor *et al* [19]	N/A	0.80	1.50	0.53
	Kim *et al* [35]	500	2.89	5.51	0.52
	Ganguly and Carmena [36]	100	2.37	2.30	1.03
	Orsborn *et al* [26]	400	1.36	1.23	1.10
	Gilja *et al* [17]	500	1.07	0.59	1.81
LFP	Flint *et al* [11]	100	N/A	N/A	0.73
	Present study (Monkey S)	400	1.27	1.31	0.97
	Present study (Monkey J)	400	1.27	1.35	0.94
ECoG	Schalk *et al* [37]	0	1.71	2.13	0.80
EEG	Wolpaw *et al* [38]	0	1.18	1.90	0.62

on the patterns of spectral power modulations evoked by the subject, and the co-occurrence of those patterns with different directions of cursor movement. Therefore, if the subject uses roughly the same control strategy each time a new decoder is trained using CLDA, then the final trained decoder parameters will end up very similar, regardless of the initialization. Furthermore, due to the high level of assistive control during the initial CLDA, the cursor initially moves accurately regardless of the decoder's initialization, thereby significantly reducing any effect of the decoder's initialization on the subject's visual feedback and resulting control strategy.

An important implication that follows from the monkeys' choice of modulated frequencies is the effect on BMI control when the number of channels used are reduced, which relates to broader questions about the range of LFP signals. Past studies have suggested that LFPs can reflect neuronal processes 0.5–2 mm away [31]. Modulations of low frequencies (8–30 Hz) have been observed across wide areas of the motor cortex [32], while ECoG studies have reported spatially specific activity at higher frequencies (>40 Hz) [12]. The correlation between channels for the different frequency bands in the current study are consistent with these previous studies—namely, low frequencies were more correlated than high frequencies across the array. Moreover, the monkeys' task performance when using varying numbers of channels for control also confirms these results, as Monkey J performed worse than Monkey S when using fewer channels due to his greater dependence on higher LFP frequencies.

4.1. Comparison of BMI performance

Development of intracortical BMIs to date have largely focused on spike activity as the only source of control input. The present study adds to a growing body of evidence that extracellular field potentials, measured through either intracortical arrays (i.e. LFP) or electrodes on the cortical surface (i.e. ECoG), are viable alternatives for BMIs. To compare the level of BMI performance reported here with that of other studies in the literature, we calculated the throughput in bits per second for various studies (see section 2). Throughput is a summary statistic that uses the mean RT and Fitts Law derived index of difficulty [33, 34], which has been proposed as a standardized assessment method for neural prostheses [28]. Table 1 compares the BMI performance achieved in this study with a sampling of other notable closed-loop BMI cursor control studies using spikes, LFPs, ECoG, and EEG. For consistency, all studies listed in the table used a 4- or 8-target center-out task, except for Flint *et al* [11] (we chose to include this study as well because it represents essentially the first demonstration of closed-loop continuous 2D control with LFPs). To calculate throughput for Monkey S and J in the present study, we used the mean RTs from their 0–80 Hz and 80–150 Hz experimental series, respectively. Due to a wide range of varying task parameters in the literature (e.g., center-out versus point-to-point reaching), it should be noted that the throughput metric is imperfect and does not allow for an exact comparison of cursor control performance across BMI studies. For instance, the calculation of the index of difficulty does not incorporate target hold time, an important aspect which undoubtedly affects the difficulty of the task (we have therefore listed the target hold time for each study as an additional indicator of task difficulty). However, despite its limitations, the throughput metric captures important aspects of target acquisition tasks such as target size, target distance, and RT, and it therefore allows us to perform approximate comparisons between studies. Overall, with respect to the throughput metric, we found that our LFP-based BMI performance compares favorably with that of spike-based studies, and exceeds the performance of other studies using LFPs, ECoG, and EEG. For an example of the center-out performance achieved with LFPs in this study, an online supplementary video is available at stacks.iop.org/JNE/11/026002/mmedia that depicts Monkey S's performance in the center-out task using the 0-80 Hz LFP range.

4.2. Practical considerations for neuroprosthetics

LFPs can potentially augment single-unit activity as control signals for neuroprosthetics to increase robustness and longevity. Our paradigm for achieving LFP-based BMI control is an important step forward toward clinically viable neuroprosthetics. We show that BMI control with LFPs can be achieved from initial arbitrary decoder parameters by using CLDA. In a similar study involving closed-loop LFP-based BMI control, Flint and colleagues recorded neural activity while the subject performed the cursor control task using

overt arm movements to train a biomimetic decoder. However, this procedure may constrain the subject to modulate neural activity in ways similar to activity evoked during natural arm movements.

Our BMI paradigm allows the decoder's parameters to be uniquely optimized for the specific types of spectral power modulations evoked by the subject during closed-loop control. Using CLDA and an assistive control paradigm, both monkeys in this study achieved proficient performance with different ranges of LFP frequencies. Such flexibility in the neural features used for closed-loop BMI control could be important for patients with deficits in their ability to volitionally modulate certain LFP frequencies.

Acknowledgments

This work was supported by the National Science Foundation Graduate Research fellowship (ALO), the American Heart Association predoctoral fellowship (ALO), the National Science Foundation CDI Type-I grant (MCG and JMC), the Defense Advanced Research Projects Agency contract N66001-10-C-2008 (JMC), and the National Science Foundation grant CBET-0954243 (JMC).

References

[1] Green A M and Kalaska J F 2011 Learning to move machines with the mind *Trends Neurosci.* **34** 61–75
[2] Fetz E E 2007 Volitional control of neural activity: implications for brain–computer interfaces *J. Physiol.* **579** 571–9
[3] Rickert J, de Oliveira S C, Vaadia E, Aertsen A, Rotter S and Mehring C 2005 Encoding of movement direction in different frequency ranges of motor cortical local field potentials *J. Neurosci.* **25** 8815–24
[4] Sanes J N and Donoghue J P 1993 Oscillations in local field potentials of the primate motor cortex during voluntary movement *Proc. Natl Acad. Sci. USA* **90** 4470–4
[5] Bansal A K, Vargas-Irwin C E, Truccolo W and Donoghue J P 2011 Relationships among low-frequency local field potentials, spiking activity, and three-dimensional reach and grasp kinematics in primary motor and ventral premotor cortices *J. Neurophysiol.* **105** 1603–19
[6] Markowitz D A, Wong Y T, Gray C M and Pesaran B 2011 Optimizing the decoding of movement goals from local field potentials in macaque cortex *J. Neurosci.* **31** 18412–22
[7] Flint R D, Ethier C, Oby E R, Miller L E and Slutzky M W 2012 Local field potentials allow accurate decoding of muscle activity *J. Neurophysiol.* **108** 18–24
[8] Flint R D, Lindberg E W, Jordan L R, Miller L E and Slutzky M W 2012 Accurate decoding of reaching movements from field potentials in the absence of spikes *J. Neural Eng.* **9** 046006
[9] Hwang E J and Andersen R A 2009 Brain control of movement execution onset using local field potentials in posterior parietal cortex *J. Neurosci.* **29** 14363–70
[10] Engelhard B, Ozeri N, Israel Z, Bergman H and Vaadia E 2013 Inducing gamma oscillations and precise spike synchrony by operant conditioning via brain–machine interface *Neuron* **77** 361–75
[11] Flint R D, Wright Z A, Scheid M R and Slutzky M W 2013 Long term, stable brain– machine interface performance using local field potentials and multiunit spikes *J. Neural Eng.* **10** 056005
[12] Schalk G, Kubánek J, Miller K J, Anderson N R, Leuthardt E C, Ojemann J G, Limbrick D, Moran D, Gerhardt L A and Wolpaw J R 2007 Decoding two-dimensional movement trajectories using electrocorticographic signals in humans *J. Neural Eng.* **4** 264
[13] Flint R, Wright Z and Slutzky M 2012 Control of a biomimetic brain–machine interface with local field potentials: performance and stability of a static decoder over 200 days *EMBC: Annual Int. Conf. of the IEEE Engineering in Medicine and Biology Society* pp 6719–22
[14] Dangi S, Orsborn A L, Moorman H G and Carmena J M 2013 Design and analysis of closed-loop decoder adaptation algorithms for brain–machine interfaces *Neural Comput.* **25** 1693–731
[15] Haykin S S 2002 *Adaptive Filter Theory* 5th edn (Englewood Cliffs, NJ: Prentice Hall) ISBN 978-0132671453
[16] Wu W, Black M J, Gao Y, Bienenstock E, Serruya M, Shaikhouni A and Donoghue J P 2003 Neural decoding of cursor motion using a Kalman filter *Advances in Neural Information Processing Systems 15* (Cambridge, MA: MIT Press) pp 133–40
[17] Gilja V *et al* 2012 A high-performance neural prosthesis enabled by control algorithm design *Nature Neurosci.* **15** 1752–7
[18] Wang W *et al* 2013 An electrocorticographic brain interface in an individual with tetraplegia *PloS one* **8** e55344
[19] Taylor D M, Tillery S I H and Schwartz A B 2002 Direct cortical control of 3D neuroprosthetic devices *Science* **296** 1829–32
[20] Gage G J, Ludwig K A, Otto K J, Ionides E L and Kipke D R 2005 Naive coadaptive cortical control *J. Neural Eng.* **2** 52–63
[21] Shpigelman L, Lalazar H and Vaadia E 2008 Kernel-ARMA for hand tracking and brain–machine interfacing during 3D motor control *Proc. Neural Information Processing System* pp 1489–96
[22] Heliot R, Venkatraman S and Carmena J M 2010 Decoder remapping to counteract neuron loss in brain–machine interfaces *EMBC: Annual Int. Conf. of the IEEE Engineering in Medicine and Biology Society* pp 1670–3
[23] Mahmoudi B and Sanchez J C 2011 A symbiotic brain–machine interface through value-based decision making *PloS one* **6** e14760
[24] Li Z, O'Doherty J E, Lebedev M A and Nicolelis M A L 2011 Adaptive decoding for brain–machine interfaces through bayesian parameter updates *Neural Comput.* **23** 3162–204
[25] Dangi S, Gowda S, Heliot R and Carmena J 2011 Adaptive kalman filtering for closed-loop brain–machine interface systems *NER: IEEE/EMBS Conf. on Neural Engineering* pp 609–12
[26] Orsborn A L, Dangi S, Moorman H G and Carmena J M 2012 Closed-loop decoder adaptation on intermediate time-scales facilitates rapid BMI performance improvements independent of decoder initialization conditions *IEEE Trans. Neural Syst. Rehabil. Eng.* A **20** 468–77
[27] Hochberg L R *et al* 2012 Reach and grasp by people with tetraplegia using a neurally controlled robotic arm *Nature* **485** 372–5
[28] Donoghue J P, Simeral J D, Kim S P, Friehs G M, Hochberg L R and Black M J 2007 Toward standardized assessment of pointing devices for brain–computer interfaces *Program No. 517.16* (San Diego, CA: Society for Neuroscience)
[29] Rouse A G, Williams J J, Wheeler J J and Moran D W 2013 Cortical adaptation to a chronic micro-electrocorticographic brain–computer interface *J. Neurosci.* **33** 1326–30

[30] Wander J D, Blakely T, Miller K J, Weaver K E, Johnson L A, Olson J D, Fetz E E, Rao R P N and Ojemann J G 2013 Distributed cortical adaptation during learning of a brain–computer interface task *Proc. Natl Acad. Sci. USA* **110** 10818–23

[31] Kajikawa Y and Schroeder C E 2011 How local is the local field potential? *Neuron* **72** 847–58

[32] Crone N E, Miglioretti D L, Gordon B, Sieracki J M, Wilson M T, Uematsu S and Lesser R P 1998 Functional mapping of human sensorimotor cortex with electrocorticographic spectral analysis: I. Alpha and beta event-related desynchronization *Brain* **121** 2271–99

[33] Fitts P M 1954 The information capacity of the human motor system in controlling the amplitude of movement *J. Exp. Psychol.* **47** 381–91

[34] MacKenzie I S 1989 A note on the information-theoretic basis of Fitts' law *J. Motor Behav.* **21** 323–30

[35] Kim S P, Simeral J D, Hochberg L R, Donoghue J P and Black M J 2008 Neural control of computer cursor velocity by decoding motor cortical spiking activity in humans with tetraplegia *J. Neural Eng.* **5** 455

[36] Ganguly K and Carmena J M 2009 Emergence of a stable cortical map for neuroprosthetic control *PLoS Biol.* **7** e1000153

[37] Schalk G, Miller K J, Anderson N R, Wilson J A, Smyth M D, Ojemann J G, Moran D W, Wolpaw J R and Leuthardt E C 2008 Two-dimensional movement control using electrocorticographic signals in humans *J. Neural Eng.* **5** 75–84

[38] Wolpaw J R and McFarland D J 2004 Control of a two-dimensional movement signal by a noninvasive brain–computer interface in humans *Proc. Natl Acad. Sci. USA* **101** 17849–54